Leading Our World In Motion

2005-01-1407

SAE TECHNICAL
PAPER SERIES

SantosTM: A New Generation of Virtual Humans

Jingzhou Yang, Tim Marler, HyungJoo Kim, Kimberly Farrell, Anith Mathai, Steven Beck, Karim Abdel-Malek and Jasbir Arora
Virtual Soldier Research (VSR) Program, Center for Computer Aided Design, The University of Iowa

Kyle Nebel
U.S. Army TACOM/RDECOM

Reprinted From: Military Vehicle Technology (SP-1962)

ISBN 0-7680-1635-5

9 780768 016352

SAE International™

**2005 SAE World Congress
Detroit, Michigan
April 11-14, 2005**

400 Commonwealth Drive, Warrendale, PA 15096-0001 U.S.A. Tel: (724) 776-4841 Fax: (724) 776-5760 Web: www.sae.org

Report Documentation Page

Form Approved
OMB No. 0704-0188

1. REPORT DATE	2. REPORT TYPE	3. DATES COVERED
APR 2005		**00-00-2005 to 00-00-2005**

4. TITLE AND SUBTITLE	5a. CONTRACT NUMBER
SantosTM: A New Generation of Virtual Humans	5b. GRANT NUMBER
	5c. PROGRAM ELEMENT NUMBER
6. AUTHOR(S)	5d. PROJECT NUMBER
	5e. TASK NUMBER
	5f. WORK UNIT NUMBER
7. PERFORMING ORGANIZATION NAME(S) AND ADDRESS(ES) **University of Iowa,Center for Computer Aided Design ,Vrtual Sodier Research Program,Iowa City,IA,52242**	8. PERFORMING ORGANIZATION REPORT NUMBER
9. SPONSORING/MONITORING AGENCY NAME(S) AND ADDRESS(ES)	10. SPONSOR/MONITOR'S ACRONYM(S)
	11. SPONSOR/MONITOR'S REPORT NUMBER(S)

12. DISTRIBUTION/AVAILABILITY STATEMENT
Approved for public release; distribution unlimited

13. SUPPLEMENTARY NOTES

14. ABSTRACT

15. SUBJECT TERMS

16. SECURITY CLASSIFICATION OF:			17. LIMITATION OF ABSTRACT	18. NUMBER OF PAGES	19a. NAME OF RESPONSIBLE PERSON
a. REPORT **unclassified**	b. ABSTRACT **unclassified**	c. THIS PAGE **unclassified**	**Same as Report (SAR)**	**16**	

ISSN 0148-7191

2005-01-1407

Santos™: A New Generation of Virtual Humans

Jingzhou Yang, Tim Marler, HyungJoo Kim, Kimberly Farrell, Anith Mathai, Steven Beck, Karim Abdel-Malek and Jasbir Arora
Virtual Soldier Research (VSR) Program, Center for Computer Aided Design, The University of Iowa

Kyle Nebel
U.S. Army TACOM/RDECOM

ABSTRACT

Presented in this paper is an on-going project to develop a new generation of virtual human models that are highly realistic in terms of appearance, movement, and feedback (evaluation of the human body during task execution). Santos™ is an avatar that exhibits extensive modeling and simulation capabilities. It is an anatomically correct human model with more than 100 degrees of freedom. Santos™ resides in a virtual environment and can conduct human-factors analysis. This analysis entails, among other things, posture prediction, motion prediction, gait analysis, reach envelope analysis, and ergonomics studies. There are essentially three stages to developing virtual humans: (1) basic human modeling (representing how a human functions independently), (2) input functionality (awareness and analysis of the human's environment), and (3) intelligent reaction to input (memory, reasoning, etc.). This paper addresses the first stage. Specifically, we discuss a new human model in terms of mechanics and appearance. We present an optimization-based approach to kinematic and dynamic motion analysis. This approach allows the avatar to operate with complete autonomy rather than with dependence on stored animations and data, or restrictions associated with inverse kinematics. With dynamic analysis, it is not necessary to solve equations of motion. A novel approach for determining reach envelopes is also presented, and this approach provides a unique tool for ergonomic studies. Methods for evaluating the physiological status of the virtual human as tasks are completed are discussed. Finally, additional on-going research is summarized. The result is an exciting step towards a virtual human that is more extensive and more complete than any other.

Keywords: Virtual humans, optimization-based model, human performance measures, real-time reaction.

INTRODUCTION

The application of virtual humans in industry is expanding, especially with respect to vehicle design and manufacturing. In fact, potential applications span a variety of areas that include the following: crash simulation (vehicular occupant injury), slip/falls (environmental injury), orthopedics (joint and tissue mechanics), gait simulation (rehabilitation), task simulation (virtual factory), and sports-performance simulation. The primary benefit of virtual humans in these areas is that they can be incorporated directly into CAD drawings. Then, engineers can perform extensive analysis concerning ergonomics and design, during the early stages of the product development process. This alleviates the need for physical mock-ups and thus shortens product design cycle times and lowers development costs.

Work on this subject spans at least two decades. Cyberman (Blackeley 1980) is an example of one of the earliest virtual humans. Chrysler Corporation developed it for the automobile industry, in order to define and analyze acceptable limb and body locations for a human model within a virtual environment. Specifically, it is used to analyze virtual drivers and passengers, and their activities in and around a car. However, Cyberman is only a simple wireframe model. Additional virtual humans of similar complexity have also been developed. *Combiman* (Bapu *et al.* 1980) was designed at the Aerospace Medical Research Laboratory in order to determine human reach capacity, and it has been used for aircraft cockpit-configuration design and evaluation. *Sammie* was designed at the University of Nottingham for general anthropometric analysis and design (Kingsley *et al*. 1981). Additional anthropometric modeling programs have been developed at the Boeing Corporation (*Boeman*, *Car*-Harris *et al.,* 1980), at Rockwell International (*Buford*– Fetter, 1982), and at the University of Pennsylvania (*Bubbleman*-Badler *et al.,*

1979). Because the appearance of initial virtual humans has been far from realistic, considerable research has been conducted in an effort to improve realism. For instance, Badler *et al.* (1993) and Thalmanns (1990, 1993, 1996) develop models based on the combination of multiple cylinders. In addition to effort focused towards visual appearance, work has been conducted with autonomous perception, intelligence, and behavior (Thalmann *et al.* 1995; Emering *et al.* 1997; Noser and Thalmann 1994, 1995, 1996; Noser 1997).

Recently, several companies have developed and marketed relatively advanced virtual-human products. Badler *et al.* (1999) created Jack™ software, which is a scalable human model with a flexible spine, and limbs that can be articulated through inverse kinematics. Jack™ can be positioned for reach analysis and visual interference analysis as well as strength, posture, and motion analysis. However, Jack™ cannot move independently, so the user must manipulate the various limbs manually. Safework™ was developed at the Ecole Politechnique (Montreal). It involves six basic mannequins that work in conjunction with an anthropometrics module to create human beings from any population. Safework™ can be used for extensive ergonomic analysis. It incorporates inverse kinematics with a full human model, which integrates with CATIA software. TechMath's Ramsis™ and Anthropos™ are human modeling systems for ergonomic analysis, design, and visualization, which are also manipulated by a user. Ramsis™ is used extensively for designing automobile interiors and airplane cockpits. Anthropos™ is a plug-in for 3D Studio with excellent visualization, ergonomic analysis.

Although the different systems mentioned above are useful, all of them are based on predetermined empirical data. Alternatively, our approach governs motion based on human performance measures that act as objective functions in an optimization problem. The above-mentioned systems require subjective manipulation and cannot quantify human performance measures, as the optimization-based approach can.

In this paper, we present newly developed facets of an optimization-based avatar that promises to be the next generation of virtual humans. This avatar is called Santos™. The work presented in this paper is part of an on-going project to develop a system with which an avatar's motion is governed by a variety of human performance measures that are incorporated in a novel optimization-based approach to posture and motion prediction. First, we introduce the human model, discussing the mechanics of skeletal motion and the details of its realistic appearance. Then, several key functionalities are presented. We also discuss the ability to receive feedback concerning the avatar's physiology. Finally, on-going research is reviewed briefly.

HUMAN MODEL

SKELETAL MODEL

In this section, we give a brief outline of the mathamtical foundation for the human skeletal model used to control the motion of Santos™. Essentially, this model relates a set of joint angles to the Cartesian coordinates of point on the avatar. A human skeleton can be modeled as a kinematic system, a series of links with each pair of links connected by single degree-of-freedom (DOF) joints as shown in Fig. 1. Therefore, a complete human body can be modeled as several open-loop chains, one of which is shown in Fig. 1.

In Fig. 1, q_i is a generalized coordinate and represents the rotation of a single basic revolute joint.

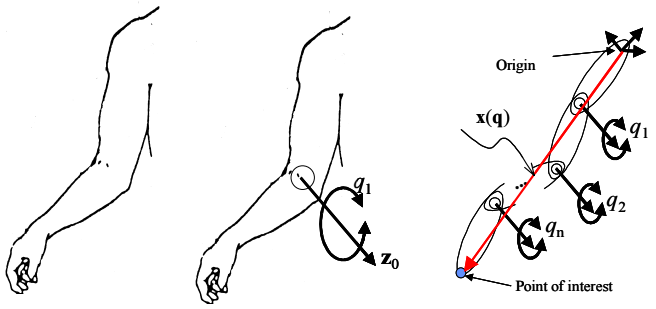

Fig. 1 Definition of a kinematic pair (e.g., a revolute joint)

Each joint in the skeletal model is represented by one, two, or three revolute joints. $\mathbf{q} = [q_1, \ldots, q_n]^T \in R^n$ is an *n*-dimensional vector of generalized coordinates, where *n* is the number of DOFs. The *end-effector* is a point on the virtual human, typically the tip of the index finger. $\mathbf{x}(\mathbf{q})$ represents the position of the end-effector in Cartesian space and is a function of the joint angles. Using the Denavit-Hartenberg (DH) method (Denavit and Hartenberg, 1955), it is determined using a series of transformation matrices as follows:

$$\mathbf{x}(\mathbf{q}) = \begin{bmatrix} x(\mathbf{q}) \\ y(\mathbf{q}) \\ z(\mathbf{q}) \end{bmatrix} = \sum_{i=1}^{i=n} [\prod_{j=1}^{j=i-1} {}^{j-1}\mathbf{R}_j]\, {}^{i-1}\mathbf{p}_i \qquad (1)$$

where $\mathbf{x} = [x \quad y \quad z]^T$. ${}^{i}\mathbf{p}_j$ and ${}^{i-1}\mathbf{R}_i$ are defined as follows:

$${}^{i-1}\mathbf{R}_i = \begin{bmatrix} \cos q_i & -\cos\alpha_i \sin q_i & \sin\alpha_i \sin q_i \\ \sin q_i & \cos\alpha_i \cos q_i & -\sin\alpha_i \cos q_i \\ 0 & \sin\alpha_i & \cos\alpha_i \end{bmatrix} \qquad (2)$$

$${}^{(i-1)}\mathbf{p}_i = [a_i \cos q_i \quad a_i \sin q_i \quad d_i]^T \qquad (3)$$

q_i is the joint angle from $\mathbf{x}_{i-1}$ axis to the $\mathbf{x}_i$ axis, d_i is the shortest distance between $\mathbf{x}_{i-1}$ and $\mathbf{x}_i$ axes, a_i is the offset distance between $\mathbf{z}_i$ and $\mathbf{z}_{i-1}$ axes, and α_i is

the offset angle from $\mathbf{z}_{i-1}$ and $\mathbf{z}_i$ axes. Details of this approach are discussed by Marler (2004).

APPEARANCE

The basic human model not only involves the skeletal mechanics, which are discussed above, but also the overall appearance, which is discussed in this section. The actual three-dimensional model is comprised of a "skin" laid over the skeleton. This "skin" can be thought of as an infinitely thin but hollow shell that defines the avatar's shape (Figs. 2 and 3).

Fig. 2 Wire frame view

Fig. 3 Solid view

Once the solid shape of the avatar is created, shaders and textures are used to provide the avatar's shape with the visual queues necessary to create the illusion of actual human skin, as shown in Fig. 4. Technically, a shader is a compilation of effects that dictate how a three-dimensional surface responds to light. Textures are two-dimensional images that are projected onto or wrapped around three-dimensional surfaces.

Fig. 4 Textured view of a virtual human

By themselves, three-dimensional models, shaders, and textures can provide convincing renderings that suggest human form, but this form cannot be manipulated until it is bound to a hierarchical joint structure representing Santos'™ skeleton (Fig. 5).

Once defined, the avatar's skin can be bound to the skeleton, allowing the avatar to be moved in a human way. Motion for the joints shown in Fig. 5 is determined using the method described in the next section and the mathematical model described above. However, to visually simulate the elasticity of real human skin as the joints are exercised, the motion of different regions of skin must be related to the motion of the skeleton. This is done using a well-known static animation technique called *skin weighting* and addresses the aesthetic issue that would otherwise cause a three-dimensional model to tear or break at the joints when joints are rotated, as shown in Fig. 6.

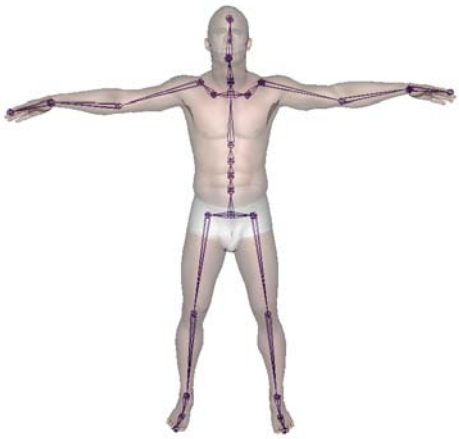

Fig. 5 Skeleton model

Fig. 6 Skin with unadjusted weight

Typically, this technique is accomplished subjectively through interactive tools – much like using a can of spray paint - that allow 8-bit gray level values to be applied to joint-specific regions of the skin. The higher the gray level value, the greater the effect a given joint has on that region (Fig. 7).

When the outer appearance of the avatar is coupled with the mathematic model (kinematic system of joints), the result is a complete human model, as shown in Fig. 8.

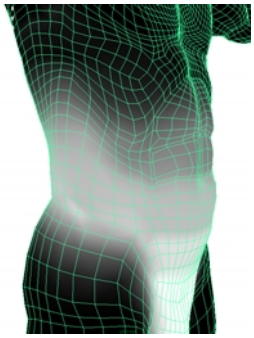

Fig. 7 Skin with adjusted weight

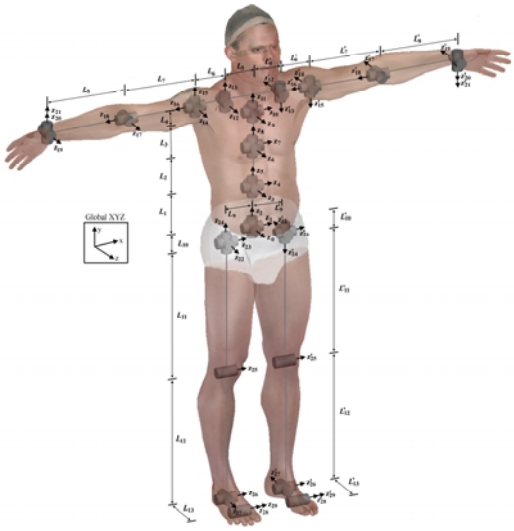

Fig. 8 Santos™, a complete virtual human

POSTURE PREDICTION

In this section, we discuss optimization-based posture prediction, which provides a cornerstone for motion prediction. An overview of the optimization formulation is presented here, while details concerning the development of the formulation are provided by Farrell and Marler (2004). In addition, the newly developed ability to control the orientation of body parts is summarized.

OPTIMIZATION PROBLEM FORMULATION

In general, the optimization problem entails finding the vector of joint angles, **q**, in order to minimize one or more human performance measures that serve as the objective functions and govern the motion of the avatar. The problem is constrained by limits on the joint angles and by the requirement that the avatar must contact the target point. The final optimization formulation is given as follows:

$$\begin{aligned} &\text{Find: } \mathbf{q} \in R^n \\ &\text{to minimize: } \textit{Human performance measure(s)} \\ &\text{subject to: } \left[\mathbf{x}(\mathbf{q}) - \mathbf{x}^{\textit{target point}}\right]^2 \le \varepsilon \\ &\qquad q_i^L \le q_i \le q_i^U;\ i = 1, 2, \ldots, n \end{aligned} \tag{4}$$

Other components of the formulation are discussed in the following sections. The problem in (4) is solved numerically using the software SNOPT (Gill *et al*, 2002), which uses sequential quadratic programming (Arora, 2004). Details concerning the different components of the optimization formulation are discussed as follows.

Design Variables and Constraints

The design variables are the generalized coordinates q_i, which represent the components of the vector **q**. These design variables have units of radians. The first constraint in (4) is the *distance-constraint*, and it requires that the end-effector contact a predetermined target point in Cartesian space, where ε is a small positive number that approximates zero. The distance between the target point and the index finger should be approximately zero. Technically, this constraint represents distance-squared. In addition, each joint angle is constrained to lie between lower and upper limits, represented by q_i^L and q_i^U respectively. These limits ensure that the avatar does not assume an unrealistic position in an effort to contact the target. They may be changed easily according to different sets of anthropologic data.

Note that the design variables are continuous and can represent infinitely many postures given a specific set of constraints (and consequent feasible space). This inherent property of the optimization problem provides a significant advantage over other approaches to human modeling. The constraints and consequent set of potential postures are essentially dictated by the avatar's environment and by the human model that the avatar represents.

Objective Functions

Various human performance measures provide the objective functions for the formulation in (4). Details concerning these performance measures are provided by Yang *et al.* (2004b). Here we present an overview. The most fundamental of these functions is *joint displacement*, which is given as follows:

$$f_{\text{JointDisp}}(\mathbf{q}) = \sum_{i=1}^{n} w_i \left(q_i - q_i^N\right)^2 \tag{5}$$

q_i^N is the *neutral position* of a joint, and $\mathbf{q}^N$ represents the overall neutral posture. The neutral posture is selected as a relatively comfortable posture, typically a standing position with arms at one's sides. A weight w_i is introduced to stress the importance of a particular joint. Currently, these weights are determined by trial and error. Generally, with joint displacement, the avatar gravitates towards the neutral position.

Effort is similar to joint displacement, but $q_i^{initial}$ replaces q_i^N and represents the avatar's initial position or starting position. Thus, when effort is used as the objective function in (4), the avatar gravitates to its starting configuration, no matter what that configuration may be. This performance measure is most significant when a series of target points are selected, with the posture changing from point to point.

Using *delta-potential-energy* as an objective function provides an alternative approach for determining the weights in (5). Various segments of the avatar's body are treated as lumped-masses. The total change in the potential energy for the masses is minimized. When determining the change in potential energy, the initial configuration is always set as the neutral position described above. In this way, the masses of the different sections of the body essentially provide inherent weights for the motion of the different segments.

Finally, *discomfort* is modeled as another variation on joint displacement. Again, the avatar moves towards the neutral position. However, this function incorporates three facets of comfort: 1) the tendency to move towards a generally comfortable position, 2) the tendency to avoid postures with which joint angles are pushed to their limits, and 3) the idea that people strive to reach or contact a point using one set of body parts at a time. Typically, in terms of upper body motion, one first tries to reach a point using one's arm. If that is unsuccessful, only then does one bend the torso. Finally, if necessary, the clavicle is extended. Note that the intent in developing this performance measure is not necessarily to quantify discomfort. Rather, the function is designed to be proportional to discomfort. Only its relative values (from one posture to another), not its absolute values, are significant.

ORIENTATION

Often, the primary concern with human modeling is the analysis of gross body motion and posture, and the only stipulation when trying to duplicate human motion concerns the position of a body part, typically a fingertip. However, when a model is required to interact with its surroundings, then the orientation of different body parts becomes critical.

Using the transformation matrices involved in the DH-method described above, we have developed a new type of constraint that can be included in (4) and controls the orientation of a particular part of the human model. The constraint essentially dictates the direction in which a local axis points (in terms of the global coordinate system) and can be used with any local coordinate system (any kinematic link). A single orientation-constraint can be used to constrain either one or two axes for a particular local coordinate system. Note that if the directions of two axes are specified, the orientation of the coordinate system is dictated uniquely. Details concerning the development and use of this new constraint are given by Marler (2004). An example is shown in Fig. 9 where both hands are touching their respective target points simultaneously and have specific orientations.

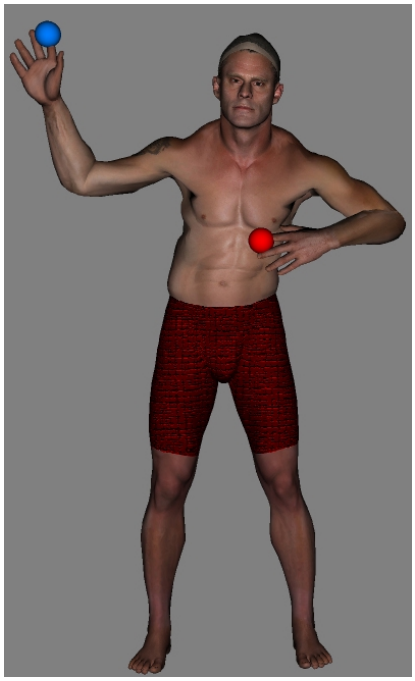

Fig. 9 Posture prediction for both hands with orientation constraints

KINEMATIC MOTION PREDICTION

While posture prediction makes it possible to evaluate the final posture of a virtual human reaching a target point, it is often important to evaluate how a virtual human moves over time to arrive at the final posture. Kinematic motion prediction computes the movement of a virtual human by determining the optimal joint values over time for each DOF. In particular, kinematic motion prediction optimizes a set of joint displacement curves while restricting the end-effector to remain on a given path in Cartesian space (Abdel-Malek *et al.*, 2004). This section discusses the general formulation of a fast approach and results in a 21-DOF model. We have

developed an optimization-based approach to kinematic motion prediction, and by carefully designing the characteristics of the B-splines used with this approach, we have achieved near-real-time performance.

OPTIMIZATION PROBLEM FORMULATION

The motion-prediction optimization problem involves finding a set of joint displacement curves $\mathbf{q}(t)$ that minimize one or more human performance measures. Conceptually, the design variables for the optimization problem are the curves that describe the joint displacements over time. Technically, we determine parameters that dictate the nature of these curves. The displacement for each joint is constrained to lie within the joint limits, at each time step. In addition, the end-effector of the virtual human is constrained to follow a discretized Cartesian path. The resulting optimization problem is formulated as follows:

Find: $P_k^i;\ k = 1, 2, \ldots, bc;\ i = 1, 2, \ldots, n$ (6)

to minimize: *Summation of human performance measure(s) evaluated at each time step*

subject to: $\left[\mathbf{x}\left(\mathbf{q}\left(t_j\right)\right) - \mathbf{x}^{path}\left(t_j\right)\right]^2 \le \varepsilon;\ j = 1, 2, \ldots ts$

$q_i^L \le P_k^i \le q_i^U;\ k = 1, 2, \ldots, bc\ ;\ i = 1, 2, \ldots, n$

where t_j is the time evaluated at time step *j*, *ts* is the number of time steps, and *bc* is the number of coefficients used in the B-spline curves. P_k^i is the k^{th} control point for the i^{th} displacement curve (B-spline curve). As with the posture-prediction problem, (6) is solved numerically using the software SNOPT (Gill *et al.*, 2002). Components of this formulation are explained as follows.

Design Variables

As opposed to the posture prediction problem, the design variables with the motion prediction problem are coefficients in B-spline curves that represent $\mathbf{q}(t)$. B-spline curves are used, because they are necessarily continuous and differentiable. In order to induce smooth and realistic motion, the joint trajectories must be at least twice differentiable; thus, it is necessary to use at least a third degree B-spline curve. Hence, the i^{th} joint trajectory is defined as follows:

$$q_i = \sum_{k=1}^{BC} \mathrm{N}_{k,3} P_k^i \qquad (7)$$

where $N_{k,3}$ is a third degree basis function that is defined recursively. There are $bc \times n$ design variables.

Constraints and Objective Functions

The first constraint in (6) is the distance constraint, which requires at each time step that the end-effector remain in contact with the given path, which is determined analytically by minimizing the jerk of the end-effector. The remaining constraints indirectly require the joint angles to remain within predetermined limits. Given inherent properties of B-splines, this is done by constraining the B-spline coefficients directly.

The objective functions are conceptually the same as they are with posture prediction. However, they are written in terms of B-splines using (7), and their value is summed over all time steps.

Note that using B-spline curves gives a result with normalized time between zero and one second. The resulting motion can be scaled to longer durations.

RESULTS

Applying the above-described algorithm to a 21-DOF model results in the motion shown in Figure 10. The end-effector follows the minimum jerk path in Cartesian space with 43 discretized points. The calculation took only 1.09 seconds on a 2.6GHz Pentium4 CPU with 512MB RAM.

Fig. 10 Superimposed time instants of motion prediction

DYNAMIC MOTION PREDICTION

In the previous section, we discuss kinematic motion prediction. However, when considering force-related issues such as walking stability, fatigue, injury, or energy consumption, it is necessary to incorporate dynamic analysis. Thus, in this section, a novel and fast optimization-based inverse dynamics method is implemented in order to predict gait-driven dynamic motion. With this approach, we provide a means of conducting gait analysis while considering externally applied loads, and the consequent model is able to adapt to changing loads. By using gradient-based

optimization software, we are to determine the optimal realistic motion with substantial speed.

Gait motion entails a typical contact problem between a foot and the environment. Generally, the contact problem raises two issues: 1) is contact between two objects; and 2) if there is contact, what are the reaction-forces at the contact points and where does the contact occur. With gait analysis, the contact forces are ground reaction forces (GRFs), and the contact points are the points at which the foot contacts the ground. Due to the uncertainty in the GRF, it is difficult to determine when the dynamic instability of falling initiates. With the current work, inverse dynamics, combined with the zero moment point (ZMP) parameter (Vukobratović and Borovac, 2004), which is discussed below, successfully addresses these questions. To accelerate the optimization process, the number and sequence of foot stepping patterns are specified, while other gait parameters such as stepping time and step length are kept flexible. A newly proposed method employing such stepping control achieves fast convergence and shows motion adaptability to external loads in push-and-gait.

DYNAMIC STABILITY USING THE ZMP

With our approach to dynamic modeling, we propose integrating the idea of dynamic stability into the optimization objective function. Thus, in this section we review the ideas behind dynamic stability.

The ZMP is an extension of the static stability parameter. As such, it incorporates gravitational forces as well as inertial forces due to motion. As long as the ZMP stays within the supporting-foot footprint (Fig. 11a), then moment equilibrium between inertial forces induced by body motion, gravity forces acting on the body, and external forces, is satisfied. In the case of bi-foot support (Fig. 11b), the ZMP should stay within the foot support region (FSR), which is a convex polygon that encloses all of the foot- ground contact points.

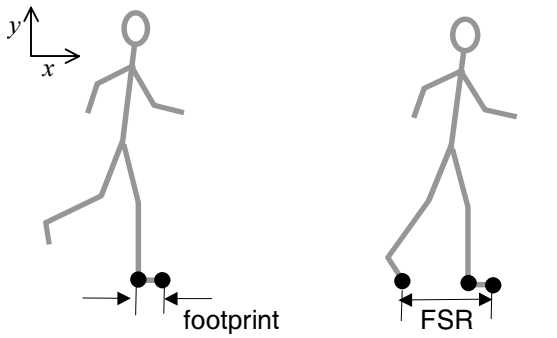

(a) single-foot support (b) bi-foot support

Fig. 11 Foot support region (FSR)

Generally, the ZMP falls within the boundary of the FSR. The concept of dynamic stability comes from the notion that a motion is more stable as the distance between the ZMP and the boundary of the FSR increases. If the ZMP is actually on the boundary of the FSR, and if its position is perturbed by external loads such that it would cross the boundary, which is physically impossible, then tipping over or falling results unless measures are taken to reposition the FSR (i.e. stepping forward or backward).

OPTIMIZATION PROBLEM FORMULATION

As does the formulation for kinematic motion prediction, the optimization formulation for dynamic motion prediction of human gait incorporates B-splines and is described as follows:

$$\text{Find: } \boldsymbol{\Theta} = \{P_k^i, \hat{t}_j\} \qquad (8)$$
$$i = 1, 2, \ldots, bc;\ k = 1, 2, \ldots, n;\ j = 1, 2, \ldots, kp$$
$$\text{to minimize: } F(\boldsymbol{\Theta}) = \int_0^T f^{DS}(\mathbf{q}(\boldsymbol{\Theta}, t), \dot{\mathbf{q}}(\boldsymbol{\Theta}, t), \ddot{\mathbf{q}}(\boldsymbol{\Theta}, t))\, dt$$
$$\text{subject to: } H^j(\boldsymbol{\Theta}) = 0;\ j = 1, 2, ..., nc$$

where $\boldsymbol{\Theta}$ is a set of design variables that includes the B-spline coefficients P_k^i and knots $\hat{t}_j$. *kp* and *nc* represent the number of knot points and the number of constraints, respectively. T is the total travel time for a gait motion. $\mathbf{q}(\boldsymbol{\Theta}, t)$ is a vector of joint-angle profiles and pelvis translations that are approximated by cubic B-spline curves as follows:

$$\mathbf{q}(\boldsymbol{\Theta}, t) = \{q_k(\boldsymbol{\Theta}, t) \mid q_k = \sum_i^{BC} P_k^i N_i(t, \hat{t}_j);\ k = 1, 2, \ldots, n\} \quad (9)$$

where $N_i(t, \hat{t}_j)$ are basis functions. $F(\boldsymbol{\Theta})$ is an objective function that measures dynamic stability. $H^j(\boldsymbol{\Theta})$ are equality constraints that incorporate constraint violations for each time step.

The pseudo-code for dynamic motion prediction using optimization-based inverse dynamics is briefly described in Fig. 12.

Stepping Pattern Control

The objective function and the constraints are implicitly governed by *stepping control*. Stepping control specifies a set of foot-points on the ground, as a function of time and knots, and is denoted by $\Psi_C(t, \hat{\mathbf{t}})$:

$$\Psi_C(t, \hat{\mathbf{t}}) = \{f \mid y_{fp}(t) = 0;\ \hat{t}_j \le t < \hat{t}_{j+1}\};\ \hat{\mathbf{t}} = \{\hat{t}_j \mid 1 \le j \le n_{knot}\} \quad (10)$$

where $y_f(t)$ is the y-coordinate of the foot-point f, and $\hat{\mathbf{t}}$ is a vector of knots.

Objective Function

Minimizing f^{DS} in (8) increases dynamic stability in two ways. First, it increases the distance between the ZMP and the border of the FSR. Secondly, it increases the span of the FSR. f^{DS} is defined as follows:

$$f^{DS}(\mathbf{q},\dot{\mathbf{q}},\ddot{\mathbf{q}},t) = (x_{ZMP}(\mathbf{q},\dot{\mathbf{q}},\ddot{\mathbf{q}}) - \xi^{m}(\mathbf{q},t))(x_{ZMP}(\mathbf{q},\dot{\mathbf{q}},\ddot{\mathbf{q}}) - \xi^{M}(\mathbf{q},t))$$
$$\xi^{m}(\mathbf{q},t) = \min[\{x_{fp}(\mathbf{q}) \mid fp \in \Psi_{C}(t,\hat{\mathbf{t}})\}] \quad (11)$$
$$\xi^{M}(\mathbf{q},t) = \max[\{x_{fp}(\mathbf{q}) \mid fp \in \Psi_{C}(t,\hat{\mathbf{t}})\}]$$

where $x_{ZMP}(\mathbf{q},\dot{\mathbf{q}},\ddot{\mathbf{q}})$ is the x-coordinate of ZMP, and x_{fp} is the x-coordinate of the foot-point f. ξ^{m} and ξ^{M} are bounds for FSR. With two dimensions, these bounds represent the minimum and maximum values for the FSR, respectively.

Begin

1) Assume initial design variables including B-spline coefficients and knots, for B-spline approximation of joint angles.
2) Calculate the joint angles and their derivatives from the design variables

Inverse Dynamics Program

3) Calculate inertial forces induced by body motion. Evaluate the objective function, constraint violations, and gradients with respect to the design variables.

Optimization Program

4) If the current point satisfies the optimality condition, stop.
5) Otherwise, predict new control parameters for joint profiles and go to step 2).

Fig. 12 Pseudo-code for optimization-based dynamics

Constraints

There are several types of constraint conditions for gait motion prediction: 1) joint-angle limits, 2) moment equilibrium, 3) foot-ground slippage, 4) foot-ground penetration, 5) foot-ground slippage condition and 6) initial/final conditions for the left foot toe.

The joint-angle limits are modeled as follows:

$$q_k^{L} \le q_k(\mathbf{\Theta},t) \le q_k^{U};\ k = 1,2,\ldots,n;\ t \in [0,T] \quad (12)$$

The condition for moment equilibrium in two-dimensions is given in inequalities as:

$$\xi^{m}(\mathbf{q},t) \le x_{ZMP}(\mathbf{q},\dot{\mathbf{q}},\ddot{\mathbf{q}}) \le \xi^{M}(\mathbf{q},t) \quad (13)$$

The constraint for preventing foot-ground slippage ensures that horizontal velocity is zero for the foot-points contacting the ground. The condition is given as follows:

$$\dot{x}_{fp}(\mathbf{q},t) = 0;\ fp \in \Psi_{C} \quad (14)$$

where $\dot{x}_{fp}$ denotes the velocity in x-direction for the foot-point fp.

The constraint for preventing ground penetration imposes the condition that the foot-points that are not in ground contact stay above ground level. This constraint is stated as follows:

$$y_{fp}(\mathbf{q},t) \ge 0;\ fp \in \Psi_{F}(t,\hat{\mathbf{t}}) \quad (15)$$

where $\Psi_{F}(=\Psi_{C}^{C})$ is a set of foot-points that do not contact the ground.

The initial/final conditions for the left foot are stated as follows:

$$x_{LFT}(\mathbf{q},t=0) = x_{IC}$$
$$x_{LFT}(\mathbf{q},t=T) = x_{FC} \quad (16)$$

where x_{LFT} is the x-coordinate of a left foot-toe. The values x_{IC} and x_{FC} are the locations at the initial/final time frame.

EXAMPLE

In this example, a 13-DOF human model is used to predict two-dimensional push-and-gait motion. There is an external force of 250 N pushing backward on the shoulder. Fig. 12 captures body postures at uniformly spaced time frames. The trunk leans forward to counter imbalance induced by the counter-clockwise moment, which is imposed by the external force on the shoulder. The arms constantly move to generate necessary inertial forces, to keep the ZMP inside the FSR. The required CPU time for optimization is 1.69 sec with a Xeon 3.06

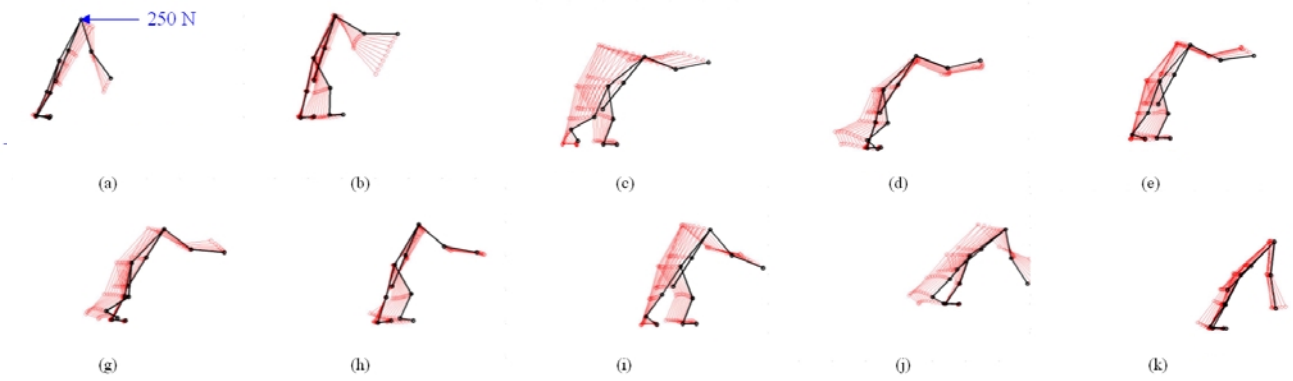

Fig. 13 Push-and-gait motion

GHz Processor. Again, SNOPT software is used for optimization. Extension to 3-dimensional analysis is on-going.

REACH ENVELOPE

The reach envelope is defined as all points the end-effector (fingertip) can touch when the virtual human moves. Reach envelopes provide an important feature for virtual humans, because if the virtual human is to accomplish a task, the target points must be inside the reach envelope. In this section, we present an analytical method for identifying the reach envelope and give an example of the reach envelope for Santos™.

In (1), $\mathbf{x}(\mathbf{q})$ represents the set of all possible points inside and on the boundary of the workspace generated by the end-effector. At a specified position in space, given by (x_p, y_p, z_p), the following vector of constraints can be written:

$$\mathbf{\Phi}(\mathbf{q}) = \begin{bmatrix} x(\mathbf{q}) - x_p \\ y(\mathbf{q}) - y_p \\ z(\mathbf{q}) - z_p \end{bmatrix} = \mathbf{0} \qquad (17)$$

Joint limits imposed in terms of inequality constraints in the form of $q_i^L \le q_i \le q_i^U$, where $i = 1, 2, \ldots, n$, are transformed into equality constraints by introducing additional generalized coordinates $\boldsymbol{\lambda} = [\lambda_1 \quad \ldots \quad \lambda_n]^T$ such that

$$q_i = \left((q_i^L + q_i^U)/2\right) + \left((q_i^U - q_i^L)/2\right)\sin\lambda_i;\ i = 1, 2, ..., n \quad (18)$$

In order to include the effect of joint limits, the vector of constraint equations $\mathbf{\Phi}(\mathbf{q})$ is augmented with the parameterized inequality constraints in (18). The resulting vector of constraints is given as follows:

$$\mathbf{H}(\mathbf{q}^*) = \begin{bmatrix} x(\mathbf{q}) - x_p \\ y(\mathbf{q}) - y_p \\ z(\mathbf{q}) - z_p \\ q_i - a_i - b_i \sin\lambda_i \end{bmatrix} = \mathbf{0};\ i = 1, 2, ..., n \qquad (19)$$

where $\mathbf{q}^* = \begin{bmatrix} \mathbf{q}^T & \lambda^T \end{bmatrix}^T$ is the new q-vector. Note that although *n* new variables λ_i have been added, *n* equations have also been added to the set of constraints.

The *Jacobian* of the constraint function $\mathbf{H}(\mathbf{q}^*)$ at a specific point $\mathbf{q}^{*0}$, is defined as the following $(3+n)\times 2n$ matrix:

$$\mathbf{H}_{\mathbf{q}^*} = \partial\mathbf{H}/\partial\mathbf{q}^* \qquad (20)$$

where the subscript denotes the variable with respect to which the derivative is taken. The matrix in (20) can be expanded as follows:

$$\mathbf{H}_{\mathbf{q}^*} = \left[\begin{array}{c|c} \mathbf{\Phi}_\mathbf{q} & \mathbf{0} \\ \hline \mathbf{I} & \mathbf{q}_\lambda \end{array}\right] \qquad (21)$$

where $\mathbf{q}_\lambda = \partial\mathbf{q}/\partial\boldsymbol{\lambda}$, $\mathbf{\Phi}_\mathbf{q} = \partial\mathbf{\Phi}/\partial\mathbf{q}$, $\mathbf{0}$ is a $(3\times n)$ zero matrix, and $\mathbf{I}$ is the identity matrix.

The reach envelope consists of surfaces defined by points in the Cartesian space at which the matrix in (21) is singular. The detailed procedure for finding these singular surfaces is provided by Yang *et al*. (2004a). The cross section of the upper extremity workspace is shown in Fig. 14. Note that inside the workspace, there are many singular surfaces inside the boundary, but we are interested in finding the boundary of the workspace only. Fig. 15 illustrates the workspace boundary for a 95% Santos™ using the right arm. To visualize the reach envelope in real-time, we have compiled a reach-envelope library for different percentile Santos™-models.

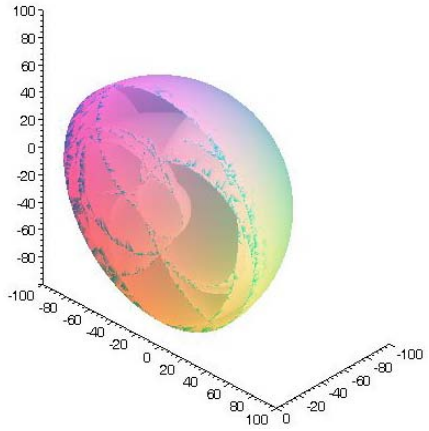

Fig. 14 Cross section of workspace for Santos'™ right arm

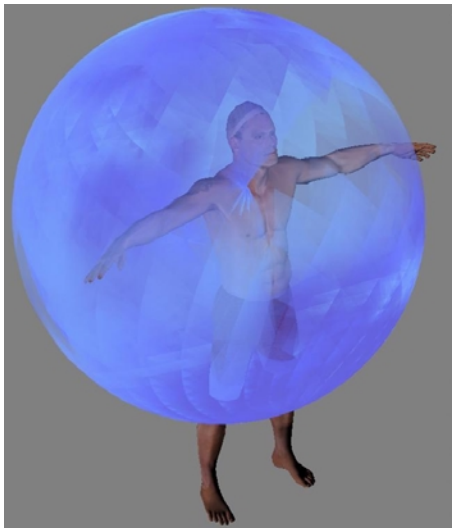

Fig. 15 Reach envelope for Santos'™ right arm

PHYSIOLOGICAL PROCESSES

In addition to predicting how a human functions in terms of motion, it is often necessary to monitor physiological aspects. Physiological systems for Santos™ consist of all the life maintaining systems that occur within a human. The initial focus has been on creating the ability to simulate the vital signs of Santos™, and significant progress has been made with the ability to model the heart rate. Thus, in this section we discuss heart rate. An overview of the physiological processes that effect heart rate is given, and this culminates in an analytical expression for actually calculating heart rate based on based on expended power.

The human body is often compared to the combustion engine, and this analogy provides a summary of what dictates the heart rate. The muscle fibers act as pistons, and adenosine triphosphate (ATP) is the gasoline. The blood, circulated by the heart, supplies the oxygen required by the ATP to produce energy. As the intensity of activity increases, more oxygen is required. Consequently, the amount of blood supplied to the muscles has to increase in order to supply the muscles with sufficient oxygen. To increase the blood supply the heart increases its stroke volume per beat and the number of beats (Astrand, 1970).

The oxygen consumed by the muscles in liberating energy is called the *oxygen uptake* (Vo_2). During physical activity, the oxygen uptake increases, and consequently the cardiac output also increases in order to keep up with the increase in oxygen uptake (Astrand, 1970). The oxygen supplied by the blood is used primarily for the aerobic portion of the power generated by the muscles and is based on the oxygen uptake response curves, which are discussed later. The heart rate is directly proportional to and can be calculated from the oxygen uptake (Margaria, 1970; Engelen *et al.* 1996). Consequently, much of the following discussion concerns oxygen uptake.

ENERGY

Understanding how the body uses energy is necessary for determining the power required by the body, which in turn, is used to calculate the heart rate. Special chemical compounds act as carriers of energy within cells. ATP is one such substance and is the cell's primary source of energy for metabolic processes. ATP breaks down into Adenosine Diphosphate (ADP) with the release of energy. The stockpile of ATP available is limited and has to be constantly regenerated. Glucose, fatty acids, and amino acids can be oxidized to produce ATP molecules. The generation of energy from ATP as well as the regeneration of ATP from ADP, lactic acid, and other waste products also requires oxygen (Astrand, 1970).

Basal Metabolic Rate (BMR)

In addition to the energy required by the muscles, the body requires energy for its functions of life, like breathing, digestion, etc. The basal metabolic rate (BMR) accounts for this energy, and is defined as the portion of human energy involved in homeostasis (merely living and breathing). This energy is exclusive of work activities, walking, standing, thinking, and digesting foods. The BMR is dependant on weight, height, age, and sex. It has units of kilocaleries/day and is calculated from the Harris-Benedict equations for men and women respectively, as follows (Frankenfield *et al.*, 2003):

$$66 + 13.75w + 5.0h + 6.76a \quad (22)$$

$$655 + 9.56w + 1.85h - 4.68a \quad (23)$$

where *a* is the age in years, *w* is the weight in kilograms, and *h* is the height in centimeters.

Although the actual basal metabolic rate varies during the course of the day, for the puprpose of calculating the heart rate, it is assumed that the BMR is constant. The BMR per second is calculated from equations (22) and (23) for a set height, weight, age, and sex, and is added to the power requirement of the body, to perform an activity. The power requirement excluding the BMR is supplied by the Santos™ energy module (Kim *et al.,* 2004).

STEADY STATE OXYGEN UPTAKE

The power to drive the physical activity ,which is derived from the sum of the power from the Santos™ energy module and the BMR, is made up of two components. The aerobic component generates energy utilizing oxygen from the blood. Alternatively, the anaerobic component does not utilize oxygen from the blood. The energy supplied during the first few seconds of an activity is almost entirely anaerobic. (Lamb, 1978). As the duration of the activity increases, as a result of ATP breakdown, the levels of Adenosine Diphosphate (ADP) in the muscles increase. This increase in ADP is the spark for aerobic metabolism to begin (Lamb, 1978). The aerobic energy process utilizes oxygen supplied by the blood, therby causing an increase in the blood supply.

Energy expenditure, including the BMR, results from the breakdown of ATP, and because ATP is replenished as the result of oxygen utilization in the mitochondria either during exercise or during recovery, there is a direct relationship between oxygen consumption and energy expenditure. Accurate measurements of the kilocalories of heat produced as the result of oxygen utilization show that normal subjects on a mixed diet of fat, carbohydrate, and protein, expend about 5Kcal of energy for each liter of oxygen they consume (Lamb, 1978). Therefore, one can obtain the oxygen uptake equivalent of power required for activity. The entire power consumed by the

body is related to an equivalent oxygen uptake by using the following relationship:

$$Vo_2^{req} = \frac{Power * 60}{20.92} \quad (24)$$

where Vo_2^{req} is the equivalent oxygen uptake value of the energy required in L/m. *Power* has units of Kilowatts, and 20.92 KJ (5Kcals) is the energy equivalent value of 1 L/min oxygen uptake. However, (24) only provides the oxygen uptake value once the body has reached the steady state. Before using steady state oxygen uptake, one must determine the oxygen update during transient periods.

TRANSIENT OXYGEN UPTAKE

The power produced in the transient stages, leading up to the steady state, is a combination of aerobic and anerobic processes. Initially the entire power requirements are met anaeorbically. At the steady state the requirements are met almost entirely from aerobic processes.

The oxygen uptake of the body does not jump directly to the steady state value but rises over time following exponential curves called response curves, corresponding to consumption of oxygen by the aerobic processes. The shape of the exponential curves and their associated time constants are different for increasing physical activity levels (also called ramp-on response curve) and decreasing physical activity levels (also called ramp-off response curve).

Physical Activity: Ramp-on

The Vo_2 response to increases in physical activity has been modeled mathematically using three exponential terms given in (25)

$$Vo_2(t) = Vo_2(b) + A_0(1 - e^{-t/\tau_0}) + A_1(1 - e^{-(t-TD_1/\tau_1)}) + A_2(1 - e^{-(t-TD_2/\tau_2)}) \quad (25)$$

Each exponential term represents a certain phase of enegetics in physical activity. $Vo_2(t)$ is the oxygen uptake response in liters/min after t seconds. $Vo_2(b)$ is the baseline oxygen uptake in liters/min. A_0, A_1, and A_2 are the asymptotic values for the exponential terms. τ_0, τ_1, and τ_2 are the time constants in seconds. TD_1 and TD_2 are the time delays in seconds, which are the time durations of time before phase 2 and phase 3 begin. The baseline oxygen uptake value is the value of the oxygen uptake when the body is at rest. This value is approximately 0.40-0.7 L/m and is dependant on body mass.

In (25), $A_0(1 - e^{-t/\tau_0})$ is the phase-1 term and starts at the onset of exercise. This phase-1 term reflects circulatory adjustments at the onset of physical activity (Barstow, 1987). The phase-1 term disappears at the start of phase-2 (after time delay TD_1) and is assigned a value of A_0' for that time. A_0' is calculated as follows:

$$A_0' = A_0(1 - e^{-TD_1/\tau_0}) \quad (26)$$

The third term of equation (25), $A_1(1 - e^{-(t-TD_1/\tau_1)})$, is called the phase-2 term, which begins after a time delay of TD_1. The primary components, phase-1 and phase-2, are relatively fast and are not affected by the muscle mass used to perform physical activity (Shunsaku *et al.*, 2001). The amplitude of the phase-2 term is set to

$$A_1' = A_0' + A_1 \quad (27)$$

The last term, $A_2(1 - e^{-(t-TD_2/\tau_2)})$, is called the phase-3 term. This term becomes significant after a time delay TD_2. The exact cause of this component is not known, but it is suspected that the serial recruitment of lower efficiency fast-twitch fibers are the cause. A model Vo_2 ramp-on response curve is shown in Fig. 16, for a subject starting from rest to his/her maximum Vo_2 value (Engelen *et al.*, 1996).

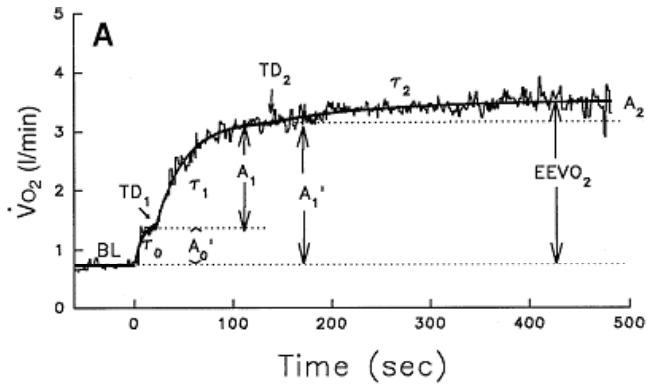

Fig. 16 Features of the three exponential model used to describe oxygen uptake during ramp-on

Physical Activity: Ramp-off

The Vo_2 response to a reduction in the level of physical activity was found to be symmetrical to the ramp-on model (Engelen *et al.*, 1996) and is provided as follows:

$$Vo_2(t) = EEVo_2 + A_0(1 - e^{-t/\tau_0}) + A_1(1 - e^{-(t-TD/\tau_1)}) + A_2(1 - e^{-(t-TD/\tau_2)}) \quad (28)$$

The only differences between (25) and (28) is that $EEVo_2$ signifies the end level of oxygen uptake from the ramp-on activity and that *TD* is a common time delay for both A_1 and A_2 exponential terms. The A_0 term is terminated after time delay *TD*. The phase-2 term has amplitude A_1', which was equal to

$$A_1' = A_0' + A_1 \quad (29)$$

The justification for this model is as follows. The two main exponential processes observed during exercise

(A_1 and A_2 from ramp on response) are present at the end of exercise. Thus, both would be present and decaying simultaneously during early recovery, when the Vo_2 requirements drop, but would reduce at different rates (Engelen *et al.*, 1996). Fig. 17 is a model ramp-off response curve (Engelen *et al.*, 1996).

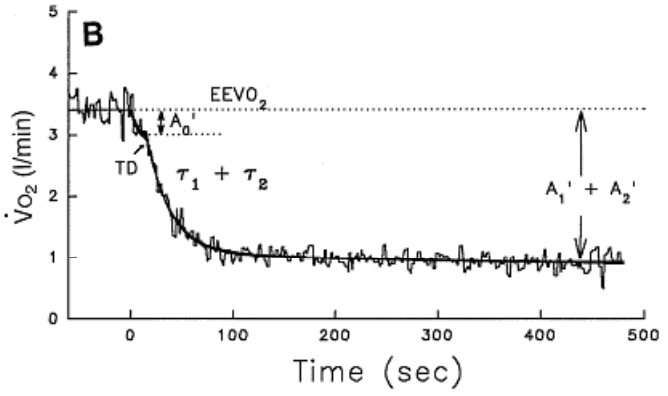

Fig. 17 Features of the three exponential model used to represent oxygen uptake ramp-off

The values the constants involved in transient oxygen uptake were taken from Engelen *et al.* (1996). The values differ for heavy activity, defined as activity above the lactic acidosis threshold (~65% max Vo_2), and light and moderate activity (<65% max Vo_2). In the case of moderate activity, the Vo_2^{req} is lower than the A_2 asymptotic value. Therefore, the third exponential term drops out, because no additional oxygen is required.

Response Curve Implementation

The above-mentioned response curves are used to simulate the changes in Vo_2. If the Vo_2 of the body needs to rise to reach the steady state, then the ramp-on curve is used. If the Vo_2 needs to fall to reach the steady state, then the ramp-off curve is used. The Vo_2 of the body is evaluated at every second, with the initial condition being the *baseline* Vo_2. The baseline Vo_2 is the minimum Vo_2 that the body needs to survive.

Three possible conditions exist concerning Vo_2 demand: an increase in the power requirement of the body, no change in the power requirement, and a decrease in the power requirement. An increase in the power requirement translates to an increased Vo_2 demand. The body has to increase its Vo_2 from the current level to the new demanded level. The current level is mapped to the matching level on the ramp-on response curve and is incremented every second following the slope of the curve until it reaches the required Vo_2 value, at which point it ceases to follow the response curve and instead maintains the steady state until a further change.

A decrease in power requirement translates into a decrease in the Vo_2 demand; the current Vo_2 level maps to its value on the ramp-off curve and follows the decaying slope until it reaches the required steady state Vo_2 value. The decrease stops once the body Vo_2 value reaches the Vo_2 required at steady state or the baseline values. The Vo_2 is not allowed to fall below the baseline value for the simulation.

STROKE VOLUME

The heart increases the stroke volume in order to pump more blood, which delivers more oxygen to keep up with the oxygen uptake (Hermansen, 1970). A relationship between the percentage maximum stroke volume and the percent maximum oxygen uptake is given as follows (Hermansen, 1970):

$$f = \frac{(32.553 + 14.291 * \mathrm{Ln}(x)) * f_{\max}}{100} \qquad (30)$$

where *f* is the stroke volume in milliliter, $f_{\max}$ is the maximum stroke volume, and x is the percentage of maximum oxygen uptake. The maximum oxygen uptake, the baseline oxygen uptake, and the maximum stroke volume are set based on the physical characteristics of the virtual human.

HEART RATE CALCULATION

The heart rate is calculated as follows (Margaria, 1970):

$$h_r = \frac{V_{o_2}}{f * H_b * (S_a - S_v)} \qquad (31)$$

where h_r is the heart rate in beats per minute, H_b is the oxygen carrying capacity of the hemoglobin in a liter of O_2 per liter of blood, S_a is the fraction of oxygenated hemoglobin in the arteries, and S_v is the fraction of oxygenated blood in the veins. H_b, S_a, and S_v are assumed to be constant for the simulation and are taken from literature (Margaria,1970).

Currently, the heart rate model has been implemented, and the development of a physiology-based objective function is being investigated. The underlying principle of this objective function is that the human body tends to optimize its energy expenditure for various activities.

SUMMARY & DISCUSSION

In this paper, we have introduced a new virtual human called Santos™. We have presented optimization-based approaches to posture prediction, motion prediction, and dynamic modeling. We have also provided new virtual-

human capabilities in terms of monitoring the body from a physiological standpoint. We have demonstrated a new approach to reach-envelope analysis. Compared to currently available virtual humans, Santos™ represents the next level in development and capabilities, and continues to grow in its ability to aid in engineering design and human study.

A primary component in the development of this virtual human has been the use of optimization. With posture prediction and kinematic motion prediction, using optimization allows the avatar to react to infinitely many scenarios. The restrictions in terms of the variety of motion that are imposed by the use of a finite library of animations and the limitations in terms of the model complexity that imposed by the use of inverse kinematics are avoided. With dynamic analysis, using optimization allows one to consider relatively complex problems with a high number of degrees of freedom, without having to solve equations of motion. This approach also results in relatively fast dynamic analysis. In fact, a key element in the development of Santos™ is the consideration of real time functionality, which is enabled by the optimization approach.

Note that although the examples pertaining to the different types of posture and motion prediction involve models with different numbers of degrees of freedom, each project aims towards a final version of Santos™ with 89 degrees of freedom. However, each project is currently in different stages of development. In this vein, the intent with this paper has been to demonstrate current capabilities and directions for additional virtual human development.

In addition to the above-mention capabilities, exciting research is on-going and concerns further features for Santos™. Using a NURBS-FEM approach, we have developed a fast method for analyzing the displacement of and stress in muscles. We are developing new approaches for modeling clothing in terms of its mechanical properties and in terms of its tendency to restrict human motion. A VICON motion capture system provides a means by which users can interact with Santos™ and can validate predicted postures and motion. In addition, validation of physiological models is being considered. An extensive 25 degree-of-freedom hand model is being developed and will be incorporated in the skeletal model discussed above. The reach-envelope capabilities are being extended in order to evaluate different zones in Santos'™ environment, in terms of potential posture-comfort. Finally, vision is being incorporated in the model as an additional human performance measure that affects posture and motion.

The emphasis with all of these projects is not just the development of a realistic mannequin. Rather, we are working towards a virtual human that looks, moves, acts, and reacts as a real human would, not just in terms of outward appearance and gross movement but also in terms of physiological functions. We strive to understand and model *how* and *why* humans act as they do. Ultimately, Santos™ will provide a design companion that essentially works with an engineer to shorten design cycle times and improve prototype development.

ACKNOWLEDGMENTS

This research is funded by the US Army TACOM project: Digital Humans and Virtual Reality for Future Combat Systems (FCS) (Contract No.: DAAE07-03-Q-BAA1).

REFERENCES

1. Abdel-Malek, K., Yang, J., Mi, Z., Patel, V.C., and Nebel, K. (2004), "Human Upper Body Motion Prediction," *The IASTED International Conference on Applied Simulation and Modeling (ASM)*, Rhodes, Greece.
2. Arora, J.S. (2004), *Introduction to Optimal Design*, 2nd ed., Elsevier, San Diego, CA.
3. Åstrand, Per-Olof, Rodahl, K. (1970), *Textbook of Work Physiology*, McGraw Hill.
4. Badler, N., O'Rourke, J., Toltzis, H. (1979), "A Spherical Representation of a Human Body for Visualizing Movement," *Proc. IEEE*, Vol. 67, No. 10, pp. 1397-1403.
5. Badler, N.I., Phillips, C.B., Webber, B.L. (1993), *Simulating Humans,* Oxford University Press.
6. Badler, N., Palmer, M.S., and Bindiganavale, R., (1999), "Animation Control for Real-Time Virtual Humans," *Comm. ACM*, Vol. 42, No. 8, pp. 64-73.
7. Bapu, P., Evans, S., Kitka, P., Korna, M., McDaniel, J. (1980), User's Guide for Combiman Programs, version 4, University of Dayton Research Institute, Dayton, Ohio.
8. Blakeley, F.M. (1980), CYBERMAN, Chrysler Corp. Detroit, Mich.
9. Denavit, J. and Hartenberg, R.S. (1955), "A Kinematic Notation for Lower-pair Mechanisms Based on Matrices," *Journal of Applied Mechanics*, Vol. 77, pp. 215-221.
10. Engelen, M., Porszasz, J., Riley, M., Wasserman, K., Maehara, K., and Barstow, T.J. (1996), "Effects of Hypoxic Hypoxia on Oxygen Uptake and Heart Rate Kinetics during Heavy Exercise," *Journal of applied physiology,* Vol. 81, No. 6, pp. 2500-2508.
11. Emering, L., Boulic, R., Balcisoy, S., Thalmann, D. (1997), "Real-Time Interactions with Virtual Agents Driven by Human Action Identification," *First ACM Conf. on Autonomous Agents'97*, Los Angeles - Marina Del Rey, pp. 476-477.
12. Farrell, K., and Marler, R. T. (2004), "Optimization-Based Kinematic Models for Human Posture," University of Iowa, Virtual Soldier Research Program, Technical Report Number VSR-04.11.

13. Fetter, W.A. (1982), "A Progression of Human Figures Simulated by Computer Graphics," *IEEE Computer Graphics and Applications*, Vol. 2, No. 9, pp. 9-13.
14. Frankenfield, D.C., Rowe, W.A., Cooney, R.N., Smith, .J. (2003), "Validation of Several Established Equations for Resting Metabolic Rate in Obese and Non-obese People," *Journal of the American Dietetic Association*, Vol. 103, No. 9, pp.1152-9.
15. Gill, P., Murray, W., and Saunders, A. (2002), "SNOPT: An SQP Algorithm for Large-Scale Constrained Optimization," *SIAM Journal of Optimization*, Vol. 12, No. 4, pp. 979-1006.
16. Harris, R., Bennett, J., Dow, L. (1980), CAR-II - A Revised Model for Crew Assessment of Reach, technical report 1400.06B, Analytics, Willow Grove, Pa.
17. Hermansen, L., Ekblom, B., Saltin, B. (1970), "Cardiac Output During Submaximal and Maximal Treadmill and Bicycle Exercise, *Journal of Applied Physiology,* Vol. 29, No. 1, pp. 82-86.
18. Kim J., Abdel-malek, K., Mi, Z., and Nebel, K. (2004), "Layout Design Using an Optimization-based Human Energy Consumption Formulation," *SAE Digital Human Modeling for Design and Engineering*, June 15-17, Rochester, Michigan.
19. Kingsley, E.C., Schofield, N.A., Case, K. (1981), "SAMMIE - A Computer Aid for Man-Machine Modeling," *Computer Graphics*, Vol. 15, No. 3, pp. 163-169.
20. Lamb, D.R. (1978), *Physiology of Exercise*, Macmillan Publishing Co.
21. Margaria, R., Cerretelli, P., Veicsteinas, A. (1970), "Estimation of Heart Stroke Volume from Blood Hemoglobin and Heart Rate at Submaximal Exercise," *Journal of Applied Physiology*, Vol. 29, No. 2, pp. 204-207.
22. Marler, R.T. (2004), "Development of an Orientation-Constraint for Human Posture-Prediction," University of Iowa, Virtual Soldier Research Program, Technical Report Number VSR-04.12.
23. Noser, H., Thalmann, D. (1994), *Towards Autonomous Synthetic Actors, in: Synthetic Worlds*, Springer, Tokyo, (T.L.Kunii, A.Luciani, eds) pp. 143-158.
24. Noser, H., Thalmann, D. (1995), "Synthetic Vision and Audition for Digital Actors," *Proc. Eurographics `95*, Maastricht, pp. 325-336.
25. Noser, H., Thalmann, D. (1996), "The Animation of Autonomous Actors Based on Production Rules," *Proc. Computer Animation '96*, IEEE Computer Society Press, pp.47-57.
26. Noser, H. (1997), "A Behavioral Animation System Based on L-systems and Synthetic Sensors for Actors," PhD Thesis, Computer Graphics Lab, LIG-DI-EPFL, CH 1015 Lausanne.
27. Shunsaku, K., Barstow,T.J., Shiojiri, T., Takaishi, T., Fukuba, Y., Kondo, N., Shibasaki, M., and Poole, D.C. **(**2001), "Effect of Muscle Mass on Vo_2 Kinetics at the Onset of Work," *Journal of applied physiology,* Vol. 90, pp. 461-468
28. Thalmann, D., Boulic, R., Huang, Z., Noser, H. (1995), "Virtual and Real Humans Interacting in the Virtual World," *Proc. International Conference on Virtual Systems and Multimedia '95*, Gifu, Japan, pp.48-57.
29. Thalmann N. M., Thalmann, D. (1990), *Computer Animation: Theory and Practice,* Springer-Verlag, Heidelberg, New York, Tokyo, (2nd edition).
30. Thalmann, N.M., Thalmann, D. (eds) (1993), *Virtual Worlds and Multimedia*, John Wiley, Chichester.
31. Thalmann N. M., Thalmann, D. (eds) (1996), *Interactive Computer Animation*, Prentice Hall.
32. Vukobratović, M., and Borovac, B. (2004), "Zero-moment Point-Thirty Five Years of Its Life," *International Journal of Humanoid Robotics*, Vol. 1, No. 1, pp. 157-173.
33. Yang, J., Abdel-Malek, K., and Nebel, K. (2004a), "Restrained and Unrestrained Driver Reach Barriers," SAE Digital Human Modeling for Design and Engineering, June 15-17, Rochester, Michigan.
34. Yang, J., Marler, R.T., Kim, H., Arora, J., and Abdel-Malek, K. (2004b), "Multi-objective Optimization for Upper Body Posture Prediction," 10th AIAA/ISSMO Multidisciplinary Analysis and Optimization Conference, August, Albany, NY.

CONTACT

Dr. Jingzhou Yang, Virtual Soldier Research (VSR) Program, Center for Computer Aided Design, The University of Iowa, Iowa City, IA 52242, Tel: 319-353-2249, Fax: 319-384-0542, E-Mail: jyang@engineering.uiowa.edu.